From the Cover: Modeling sporadic loss of heterozygosity in mice by using mosaic analysis with double markers (MADM)

Mandar Deepak Muzumdar, Liqun Luo, and Hui Zong

PNAS 2007;104;4495-4500; originally published online Mar 5, 2007;
doi:10.1073/pnas.0606491104

Modeling sporadic loss of heterozygosity in mice by using mosaic analysis with double markers (MADM)

Mandar Deepak Muzumdar*†, Liqun Luo†‡, and Hui Zong†§

†Howard Hughes Medical Institute and Department of Biological Sciences and *School of Medicine, Stanford University, Stanford, CA 94305

Edited by Kathryn V. Anderson, Sloan–Kettering Institute, New York, NY, and approved November 20, 2006 (received for review September 7, 2006)

The initiation and progression of many human cancers involve either somatic activation of protooncogenes or inactivation of tumor-suppressor genes (TSGs) in sporadic cells. Although sporadic gain-of-function of protooncogenes has been successfully modeled in mice [e.g., Johnson L, Mercer K, Greenbaum D, Bronson RT, Crowley D, Tuveson DA, Jacks T (2001) *Nature* 410:1111–1116], generating a similar degree of sparseness of TSG loss-of-function remains a challenge. Here, we use mosaic analysis with double markers (MADM) to achieve TSG inactivation and concurrent labeling in sporadic somatic cells of mice, closely mimicking loss of heterozygosity as occurs in human cancers. As proof of principle, we studied the consequence of sporadic loss of p27kip1, a cyclin-dependent kinase inhibitor. MADM-mediated loss of p27kip1 results in mutant cell expansion markedly greater than that observed in conventional *p27kip1* knockouts. Moreover, the direct comparison of WT and mutant cells at single-cell resolution afforded by MADM reveals that p27kip1 regulates organ size *in vivo* by cell-autonomous control of cell cycle exit timing. These studies establish MADM as a high-resolution method for modeling sporadic loss of heterozygosity in mice, providing insights into TSG function.

cell proliferation | development | knockout | tumor suppressor genes

Human cancers frequently result from biallelic inactivation of a tumor-suppressor gene (TSG) (1, 2). The first inactive TSG allele may be acquired through inheritance or a mutagenic event. The loss of the remaining functional TSG allele through loss of heterozygosity (LOH) in sporadic cells promotes tumorigenesis (3). To model this phenomenon in mice, it would be ideal to limit gene inactivation to a small number of cells, preferably one, and to unambiguously distinguish mutant cells from surrounding cells. In mouse experimental models, sporadic LOH can, in theory, be achieved by using conditional knockout methods, in which a tissue-specific Cre recombinase excises loxP-flanked genes ("floxed") through intrachromosomal recombination (Fig. 1*A Left*) (4). These knockout cells can be visualized by concomitantly introducing an independent Cre reporter transgene that expresses a marker gene (e.g., GFP) (5) upon Cre-mediated recombination. However, low-frequency gene knockout is difficult to achieve with this method, and the stochastic nature of two independent recombination events (6) does not guarantee 100% correlation between labeling and knockout [Fig. 1*A Left*, arrow and arrowhead; other strategies of visualizing mutant cells have other caveats (7)]. In contrast, the mosaic analysis with double markers (MADM) system achieves simultaneous gene inactivation and specific labeling of mutant cells through a single Cre/LoxP-mediated interchromosomal mitotic recombination event [Fig. 1*A Right* and supporting information (SI) Fig. 5*A*] (7). Moreover, recombination occurs infrequently (ranging from $<0.001\%$ to $\approx 1\%$ of cells depending on which Cre line is used) (7), allowing sporadic gene knockout.

The MADM cassettes have been inserted into the *ROSA26* locus on mouse chromosome 6 (7). By design, if a gene of interest is distal (telomeric) to *ROSA26* and its mutant allele is recombined with the GR transgene, G_2-X recombination in dividing cells (SI Fig. 5*A Top*, left branch) generates a green homozygous mutant cell and a red homozygous WT cell (Fig. 1*B*). Conversely, if the mutant allele is recombined with the RG transgene, G_2-X recombination generates a red mutant cell and a green WT cell (Fig. 1*C*). G_0, G_1, or G_2-Z recombination events create yellow cells heterozygous for the gene of interest (SI Fig. 5*A Bottom*; top, right branch). Until now, the ability of MADM for simultaneous gene knockout and cell labeling had not yet been experimentally established.

As proof of principle for modeling sporadic LOH, we used MADM to analyze the consequence of inactivation of *p27kip1* (*p27*), located distal to *ROSA26* on chromosome 6. *p27* encodes a cyclin-dependent kinase inhibitor (CKI) that functions at the G_1/S transition of the cell cycle (8, 9). Loss of p27 protein correlates with poorer prognosis in a number of human cancers (10, 11), suggesting its role in tumor suppression. Moreover, *p27* knockout mice exhibit a 30% increase of body size and multiorgan hyperplasia (9). Here, we report that MADM indeed permits simultaneous knockout and labeling of sporadic cells in mice. Furthermore, sporadic knockout of *p27* results in a multifold increase in cell number far exceeding that observed in conventional knockout mice. Finally, we present *in vivo* evidence that p27 limits cell expansion by regulating cell cycle exit timing rather than cell cycle length.

Results and Discussion

MADM Predictably Labels Homozygous Mutant and WT Cells in Mosaic Mice. We focused our study on the early postnatal cerebellar granule cell lineage. During normal development, granule cells are generated through postnatal expansion of granule cell progenitors in the outer external granular layer (EGL), a process that ends at approximately postnatal day 21 (P21) (12). In P7 WT mice, immunostaining reveals the presence of Ki67-positive, dividing cells in the outer EGL and the abrupt increase of p27 protein in the inner EGL, where granule cells have exited the cell cycle (Fig. 1*D*). p27 expression is sustained in postmitotic granule cells of the internal granule layer (IGL), where granule cells ultimately reside after they migrate across the molecular layer. We first tested whether MADM-mediated G_2-X recombination results in loss of p27 protein expression in specifically labeled cells, as predicted by Fig. 1 *B* and *C*. We recombined a *p27* null allele (9) with the GR transgene and introduced into the

Author contributions: M.D.M. and H.Z. contributed equally to this work; M.D.M., L.L., and H.Z. designed research; M.D.M. and H.Z. performed research; M.D.M., L.L., and H.Z. analyzed data; and M.D.M. and H.Z. wrote the paper.

The authors declare no conflict of interest.

This article is a PNAS direct submission.

Freely available online through the PNAS open access option.

Abbreviations: EGL, external granular layer; IGL, internal granular layer; LOH, loss of heterozygosity; MADM, mosaic analysis with double markers; P*n*, postnatal day *n*; TSG, tumor-suppressor gene.

See Commentary on page 4245.

‡To whom correspondence should be addressed. E-mail: lluo@stanford.edu.

§Present address: Department of Biology, 1210 University of Oregon, Eugene, OR 97403-1210.

This article contains supporting information online at www.pnas.org/cgi/content/full/0606491104/DC1.

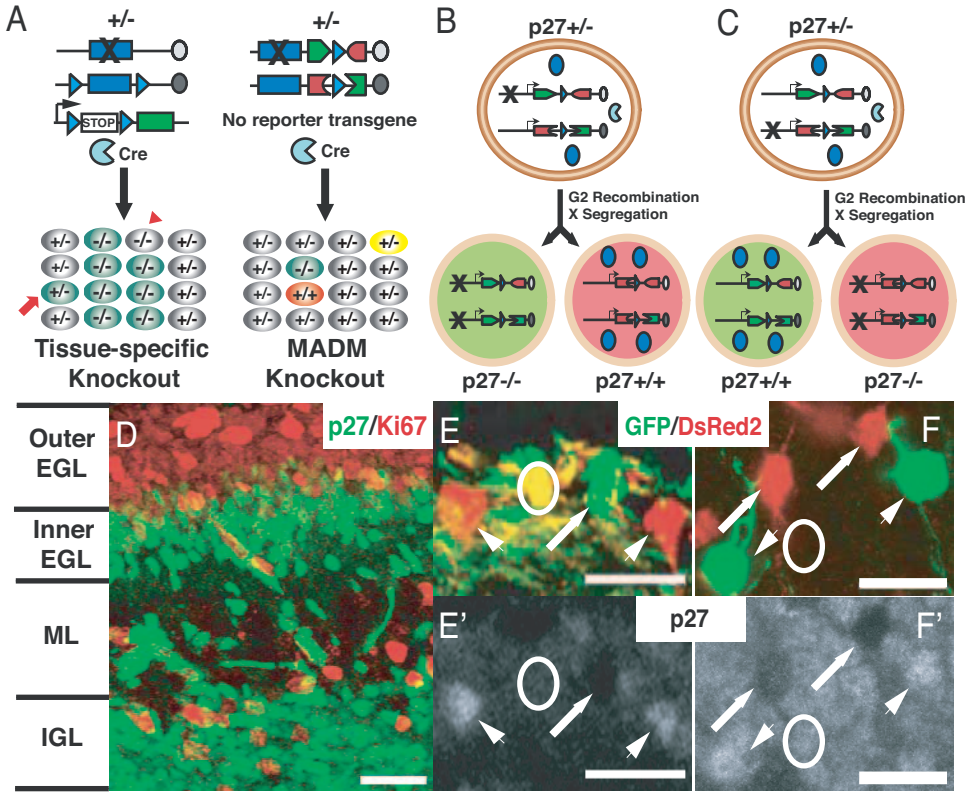

Fig. 1. Sporadic loss of heterozygosity of *p27* in MADM mice. (*A*) Schematic representation of conditional genetic approaches to study LOH of TSGs in mice. Tissue-specific knockouts (*Left*) use Cre/LoxP-mediated intrachromosomal recombination of a floxed conditional TSG allele in a tissue or cell-type-specific manner. Concurrent inclusion of an independent Cre-dependent reporter (e.g., loxP-stop-loxP-GFP) would result in heterozygous cells that are labeled (arrow) and homozygous mutant cells that are not labeled (arrowhead), when a low efficiency Cre transgene is used. Greater sporadicism and predictable labeling is achieved with MADM (*Right*) by interchromosomal G_2-X recombination events. Blue rectangles correspond to TSG alleles. ''X'' corresponds to mutant allele. Light blue triangles represent LoxP sites (targets of Cre recombinase). Gray ovals represent centromeres. See SI Fig. 5 for details of the MADM scheme and origin of yellow cells. (*B*) GR-MADM: schematic representation of LOH by using MADM in which a mutant TSG allele is telomeric to the GR transgene on the same chromosomal arm. G_2-X mitotic interchromosomal recombination results in a GFP-labeled homozygous mutant cell and a sister DsRed2-myc-labeled WT cell. ''X'' corresponds to mutant TSG alleles. Blue circles denote TSG protein. (*C*) RG-MADM. Schematic representation of LOH by using MADM in which a mutant TSG allele is telomeric to the RG transgene on the same chromosomal arm. G_2-X mitotic interchromosomal recombination results in a DsRed2-myc-labeled mutant cell and a sister GFP-labeled homozygous WT cell. (*D*) *p27* is highly expressed in postmitotic ($Ki67^-$) granule cells of the EGL and IGL of the postnatal cerebellum (here, shown at postnatal day 7). Dividing ($Ki67^+$) granule cell progenitors are situated in the outer EGL. Sporadic $Ki67^+$ cells outside the outer EGL most likely represent dividing progenitors of other cerebellar cell types. (*E* and *E′*) In *p27* GR/RG;Hprt-Cre (GR-MADM) mice, p27 protein is absent in green granule cells (arrows) and increased in red cells (arrowheads) compared with heterozygous yellow cells (circle) in the inner EGL of the cerebellum. (*F* and *F′*) In *p27* RG/GR;Hprt-Cre (RG-MADM) mice, p27 is absent in red granule cells (arrows) and increased in green cells (arrowheads) compared with surrounding heterozygous cells (circle) in the IGL of the cerebellum. See SI Fig. 6 for more examples. [Scale bars: 20 μm (*D*) and 10 μm (*E* and *F*).]

same mice the RG transgene and a ubiquitously expressed Hprt-Cre transgene (13) (*p27* GR/RG;Hprt-Cre, hereafter referred to as GR-MADM; Fig. 1*B* and SI Fig. 5*B*). In parallel, we also generated *p27* RG/GR;Hprt-Cre mice (hereafter referred to as RG-MADM; Fig. 1*C*). As predicted in GR-MADM mice (Fig. 1*B*), p27 protein is absent in green (homozygous mutant) cells but more abundant in red (homozygous WT) cells than the surrounding yellow and colorless cells (heterozygous; Fig. 1 *E* and *E′*). Conversely, in RG-MADM mice (Fig. 1*C*), red cells lack p27 protein, whereas green cells express higher levels of p27 protein (Fig. 1 *F* and *F′*). These observations were confirmed by careful examination of >100 MADM-label cells (e.g., SI Fig. 6). These experiments demonstrate that MADM can achieve gene knockout in sporadic cells and predictably label them with its engineered markers.

Cell-Autonomous Loss of *p27* Results in Greater Cell Number Expansion. Conventional *p27* knockout mice exhibit a 70% increase in the number of cerebellar granule cells (14). However, LOH naturally occurs in sporadic cells rather than throughout entire tissues. Moreover, conventional knockout precludes analysis of the cell autonomy of gene function. Given the infrequency of interchromosomal recombination, MADM leads to simultaneous gene knockout and labeling in sporadic cells (Fig. 1*A* and ref. 7). Using this feature, we determined whether sporadic loss of *p27* leads to a similar hyperplastic phenotype. Qualitatively, MADM-mediated sporadic knockout results in obvious expansion of mutant granule cells (Fig. 2 *B* and *C*; SI Fig. 6) compared with WT controls (Fig. 2*A*). To quantify this effect, we made use of $p27^{+/+}$ sibling cells that are generated simultaneously with $p27^{-/-}$ cells but are labeled with different markers in the same animal (Fig. 1 *B* and *C*). We assessed the difference of cell expansion by calculating the mutant-to-WT cell number ratio in systematically sampled cerebellar sections (see *Materials and Methods*) at the completion of granule cell development. As shown in Fig. 2*D′*, the ratio between green and red cells in GR/RG;Cre (WT-MADM) mice is not significantly different from 1 (green/red ratio of 1.49 ± 1.37, 95% confidence interval), revealing equal expansion potential between WT sibling cells. However, the mutant/WT ratio increases to ≈6 in GR-MADM granule cells (Fig. 2 *D* and *D′*). This experiment demonstrates that p27 negatively regulates cell expansion *in vivo*, consistent

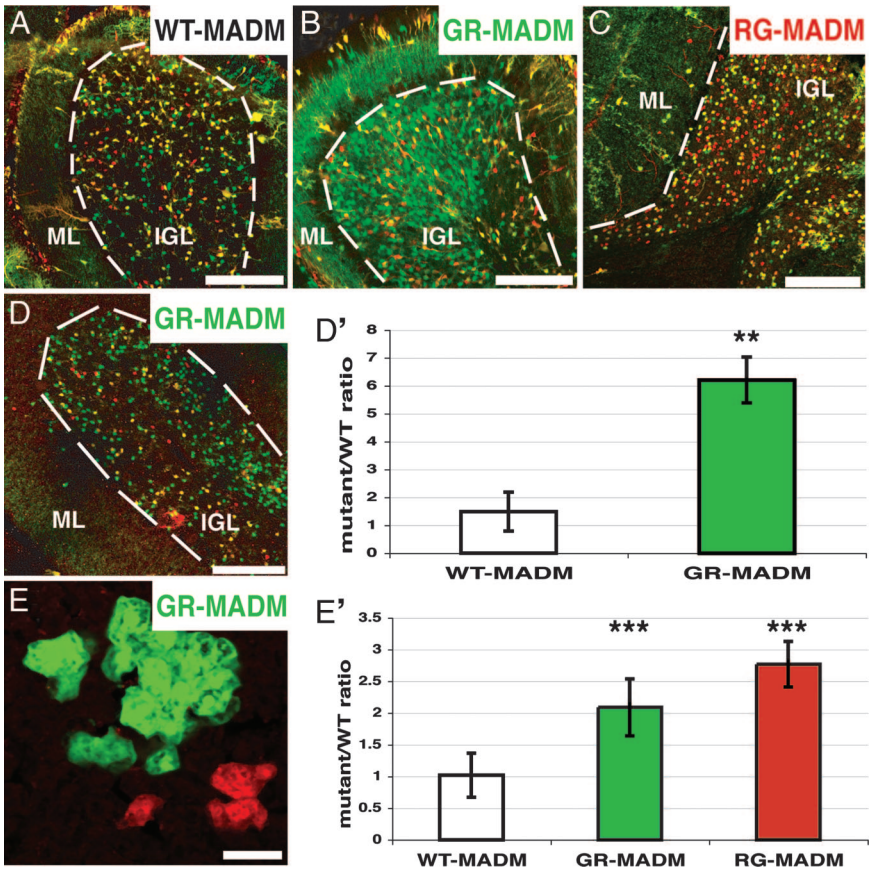

Fig. 2. Cell-autonomous loss of *p27* results in greater cell number expansion. (*A*) Sagittal section of a P30 cerebellum in a GR/RG;Hprt-Cre (WT-MADM) mouse, showing qualitatively equivalent numbers of red and green granule cells in the IGL. (*B*) Sagittal section of a P30 cerebellum in a *p27*,GR/RG;Hprt-Cre (GR-MADM) mouse, showing a marked expansion of green compared with red granule cells in the IGL. Green staining in the molecular layer corresponds to the axons of MADM-labeled granule cells. (*C*) Sagittal section of a P28 cerebellum in *p27* RG/GR;Hprt-Cre (RG-MADM) mouse, showing a marked expansion of red compared with green granule cells in the IGL. The lack of red staining in the molecular layer (ML) occurs because DsRed2-myc does not stain well in granule cell axons. (*D* and *D'*) Representative sagittal section of a single folia of a P22 cerebellum in a *p27* GR/RG;Wnt1-Cre mouse, sampled for quantification of granule cell expansion in the cerebellum (see *Materials and Methods*). Each column represents the average mutant-to-WT ratio (±SEM) for individual mice ($n = 9$ for WT-MADM, $n = 6$ for GR-MADM). **, $P = 0.002$. (*E* and *E'*) Representative hepatocyte twinspot from a P30 GR-MADM mouse, sampled for quantification of hepatocyte expansion in the liver. Each column represents the average mutant-to-WT ratio (±SEM) for individual twinspots ($n = 20$–30) from WT-MADM, GR-MADM, and RG-MADM mice. ***, WT-MADM vs. GR-MADM, $P < 0.001$. ***, WT-MADM vs. RG-MADM, $P < 0.0001$. [Scale bars: 100 μm (*A–D*) and 25 μm (*E*).]

with its characterized function as a G_1 cyclin-dependent kinase inhibitor (8). Importantly, the cell expansion phenotype manifested in MADM-mediated sporadic knockouts is much more drastic than the 70% increase of granule cell number in conventional knockouts (14).

To test whether this greater cell number expansion applies to other tissues, we examined the consequence of sporadic loss of *p27* in hepatocytes of the liver. In both GR-MADM and RG-MADM mice, we analyzed clusters of green and red cells that are adjacent to each other (twinspots; Fig. 2*E*). These cells most likely represent progeny from the same recombination event, because liver cells do not undergo extensive migration later in development (15). Compared with WT-MADM clones, which have a ratio of ≈1 between red and green cells (Fig. 2*E'*, left column), the ratio of $p27^{-/-}$ cells over $p27^{+/+}$ cells is >2 regardless of whether mutant cells are labeled green (GR-MADM) or red (RG-MADM; Fig. 2*E'*, center or right columns). Moreover, the mutant/WT ratio of GR-MADM and RG-MADM mice is not significantly different ($P > 0.10$), suggesting that fluorescence marker expression does not affect the cell-expansion phenotype. An unbiased analysis of whole-liver sections also yields comparable mutant/WT ratios (see *Materials and Methods*). Our results demonstrate that the mutant hepatocyte number rises by 110–180% compared with WT cells, whereas hepatocyte number increases by only 60% in conventional knockouts (9). Therefore, sporadic *p27* knockout by MADM consistently generates a more extreme cell expansion phenotype than conventional knockouts in different organs.

The difference of cell expansion between organismal and sporadic knockout can be explained by a few possible mechanisms. First, given the small proportion of mutant cells in MADM mice, sporadic expansion may evade global organ size-control mechanisms. Observations of mice after partial hepatectomy support the existence of such global mechanisms in liver-size determination (16, 17). Second, whereas conventional knockouts reveal the consequence of chronic loss of gene function, MADM-mediated conditional mutagenesis permits acute knockout at a later point in development, an event that may lead to different phenotypes because of lack of compensation (18). Finally, interactions between MADM-generated sporadic mutant cells and their heterozygous neighbors may allow greater mutant cell expansion than in a situation where every cell is mutant. Regardless, the phenotypes observed in MADM knockouts should more closely recapitulate the consequence of sporadic TSG inactivation as occurs in human cancers.

Expansion of $p27^{-/-}$ Cells Results from a Delay in Cell Cycle Exit. We next explored how p27 controls organ size *in vivo*. As suggested

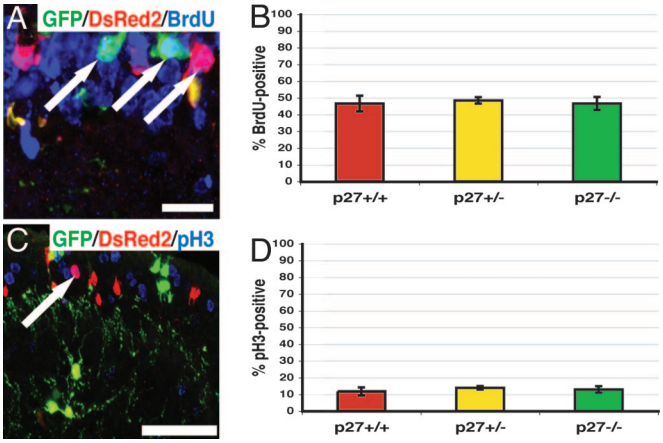

Fig. 3. No detectable change in the cell cycle profile of $p27^{-/-}$ cells. (*A*) Representative example of BrdU-positive (arrows) and BrdU-negative green ($p27^{-/-}$), red ($p27^{+/+}$), and yellow ($p27^{+/-}$) cells in the outer EGL of a P4 GR-MADM cerebellum. (*B*) Quantification of the proportion of green, red, and yellow cells described in *A* that are BrdU-positive. Each column represents the average percentage of BrdU-positive cells of each genotype (±SEM; $n = 4$ mice). (*C*) Representative example of phospho-Histone-3 (pH3) positive (arrow) and pH3-negative green ($p27^{-/-}$), red ($p27^{+/+}$), and yellow ($p27^{+/-}$) cells in the outer EGL of a P4 GR-MADM cerebellum. A lower-magnification view is shown than in *A* to demonstrate the sparser labeling of pH3 compared with BrdU. (*D*) Quantification of the proportion of green, red, and yellow cells described in *C* that are pH3-positive. Each column represents the average percentage of pH3-positive cells of each genotype (±SEM; $n = 4$). [Scale bars: 10 μm (*A*) and 50 μm (*C*).]

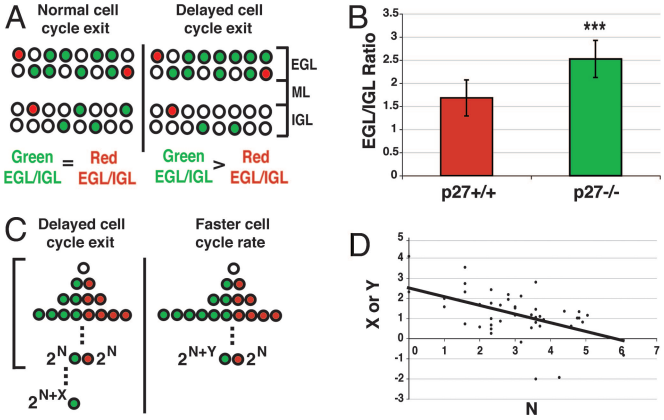

Fig. 4. Expansion of $p27^{-/-}$ cells results from a delay in cell cycle exit. (*A*) Rationale for analysis of cell cycle exit timing of granule cells in the cerebellum. See *Results and Discussion* for details. Green cells represent $p27^{-/-}$, and red cells represent WT. (*B*) Quantification of the EGL/IGL ratio of green ($p27^{-/-}$) and red ($p27^{+/+}$) cells of P4 GR-MADM mice. Colored bars represent average EGL/IGL ratios (±SEM) for individual mice ($n = 10$). ***, $P < 0.001$. (*C*) Rationale for analysis of cell cycle exit timing of hepatocytes in the liver. See *Results and Discussion* for details. Green cells represent $p27^{-/-}$, and red cells represent WT. Bracket notes normal time window of cell division. (*D*) Graph represents plot of X or Y (extra mutant cell divisions) vs. N (WT number of cell divisions) ($n = 49$ twinspots) from P30 GR-MADM and RG-MADM mice. X or Y and N were determined with the following formulas: X or Y = $\log_2$ (mutant cell number/WT cell number); $n = \log_2$ (WT cell number in twinspot). Regression line is shown. Correlation is not positive ($R^2 = 0.256$, $P = 0.0002$).

previously (19), decreased apoptosis may lead to the expansion of $p27^{-/-}$ cells. To examine whether decreased apoptosis contributes to $p27^{-/-}$ granule cell expansion, we performed immunostaining for cleaved (active) caspase-3. We find that cell death occurs very infrequently during granule cell expansion (data not shown), consistent with a previous report (20). Moreover, we rarely observe the presence of active caspase-3 in MADM-labeled cells regardless of genotype (SI Fig. 7*A* and Fig. 7*A′*). These data suggest that the expansion of $p27^{-/-}$ cells is not because of decreased apoptosis.

Previous studies have suggested two different mechanisms that promote increased proliferation of $p27^{-/-}$ cells. Because p27 functions as a cyclin-dependent kinase inhibitor at the G_1/S transition (8), its loss could result in a shortened G_1 phase, leading to an increase in cell cycle rate (19, 21). On the other hand, a delay in cell cycle exit permits prolonged expansion and thus increased proliferation (22, 23). To assess the contributions of these two mechanisms *in vivo*, we performed quantitative comparisons of mutant and WT cells within the same mosaic animal using MADM. In the G_1 shortening model, one would expect an increased proportion of cells in other cell cycle phases. To test this hypothesis, we determined the proportion of colored cells labeled with a pulse of bromodeoxyuridine (BrdU, S phase marker) or phospho-Histone 3 (pH3, M phase marker) in GR-MADM mice at P4, a time point when most granule cell progenitors are proliferating. We find that the proportion of $p27^{-/-}$ (green), $p27^{+/-}$ (yellow), and $p27^{+/+}$ (red) cells in the S phase (46–49% of cells) and M phase (10–12%) is equivalent (Fig. 3), suggesting no significant G_1 shortening due to *p27* loss.

To test whether $p27^{-/-}$ cells exhibit a delay in cell cycle exit, we took advantage of the stereotypical developmental process of granule cell progenitors in which dividing cells reside in the EGL, whereas postmitotic granule cells situate in the IGL. We compared the number of $p27^{-/-}$ and $p27^{+/+}$ cells in the EGL and IGL of GR-MADM mice at P4, when some granule cells begin to differentiate. If cell cycle exit timing is unperturbed, the EGL-to-IGL ratio (EGL/IGL) of mutant cells should be equivalent to that of WT cells. If cell cycle exit timing is delayed because of p27 loss, mutant cells should remain longer in the EGL and undergo extra divisions, leading to a higher EGL/IGL ratio for mutant cells in comparison with WT cells (Fig. 4*A*). Indeed, in MADM mosaics, we observe the latter (Fig. 4*B*), suggesting a delay in cell cycle exit of $p27^{-/-}$ cells. An alternative interpretation of an increased EGL/IGL ratio could be that $p27^{-/-}$ cells differentiate on time but fail to migrate out of the EGL, similar to the role of p27 in cortical neuronal migration (24). Two observations argue against this possibility. First, EGL $p27^{-/-}$ cells express the proliferative marker Ki67 (SI Figs. 7*B* and 7*B′*), implying that they are still dividing rather than simply failing to migrate after cell cycle exit. Second, $p27^{-/-}$ cells ultimately migrate to the IGL and express appropriate differentiation markers (SI Figs. 7*C*–7*D′*) but outnumber $p27^{+/+}$ cells in adults (Fig. 2*D′*), an outcome that would not result from a simple migration defect.

We also performed a quantitative analysis to determine whether p27 similarly mediates cell cycle exit in developing hepatocytes. After a recombination event in a dividing hepatocyte progenitor, each daughter cell normally undergoes n cell divisions (in a symmetric mode as suggested by the equal number of red and green cells in WT-MADM; Fig. 2*E′*) to produce 2^n cells. In a delayed cell cycle exit model, $p27^{-/-}$ daughter cells would undergo X extra cell divisions to generate 2^{n+X} cells. X should not vary with n. In a faster cell cycle rate model, $p27^{-/-}$ daughter cells would undergo Y extra cell divisions to generate 2^{n+Y} cells in the same period in which their WT siblings produce 2^n cells. In this case, Y should be proportional to n (Fig. 4*C*). An analysis of hepatocyte twinspots reveals that there is no positive correlation between X or Y and n (Fig. 4*D*), ruling out a faster cell cycle rate model. Thus, loss of *p27* appears to result in a delay in cell cycle exit leading to overproliferation of both cerebellar granule cells and hepatocytes. The degree of mutant cell expansion of granule cells (6-fold, i.e., two to three extra cell divisions) is greater than that of hepatocytes (≈2.5-fold i.e., one to two

extra cell divisions), implying that p27 plays a more significant role in cell cycle exit timing in granule cells.

Our findings suggest that p27 controls the precise timing of cell cycle exit, an important mechanism in organ-size control. Although such a role has been suggested from previous *in vitro* studies of mammalian cells (14, 23) or during *Drosophila* embryonic development (22), our work adds clear *in vivo* evidence supporting this notion in mammalian neural tissue and hepatocytes. In some cases, studies of certain tissues that have synchronized developmental timing, including the organ of Corti (25), ovarian follicles (26), and the retina (27), suggest the involvement of p27 in controlling cell cycle exit in mice. However, the MADM system allows the study of all of the other cell types that do not fall into this category. Moreover, mosaic analysis demonstrates that this function of p27 is cell-autonomous. The importance of sporadic knockout for studies of cell autonomy is also supported by another observation. All conventional $p27^{-/-}$ mice develop pituitary adenomas of the pars intermedia by 10 weeks of age (9). However, human pituitary tumors primarily originate from the pars distalis and do not exhibit LOH of *p27* (28). We examined five pituitaries of GR-MADM and RG-MADM mice (>10 weeks old) and never found clonal expansion of labeled $p27^{-/-}$ cells (data not shown). This observation suggests that a non-cell-autonomous mechanism might be responsible for the formation of pituitary adenomas in conventional $p27^{-/-}$ mice.

Use MADM for LOH Modeling. Our study confirms the use of the MADM system for gene knockout and predictable labeling in sporadic cells, making it a superb genetic tool for modeling sporadic LOH in mice. There are several appealing features of the MADM system. It guarantees 100% correlation between labeling and genotype, allowing unambiguous phenotypic analysis with single-cell resolution, which enables the study of cell-autonomous functions of tumor-suppressor genes and the interactions between mutant cells and their microenvironment. Furthermore, labeled WT siblings of mutant cells serve as an *in situ* control, which greatly simplifies phenotypic analysis. Using this feature, we have provided definitive evidence for the *in vivo* function of p27 in controlling cell cycle exit timing. Overall, MADM allows the study of immediate-early events upon TSG loss, which should shed light on the initial phases of tumorigenesis. Combined with rapid advances in optical imaging techniques (29, 30), MADM will also permit tracing of mutant cell behavior in a natural setting. Moreover, screening for novel recessive TSG mutations has remained a great challenge for the cancer field. As a genetic mosaic system, MADM makes recessive genetic screens much more feasible (31) and should lead to the identification of novel TSGs. Finally, in conjunction with the international consortium to make null alleles of every gene in the mouse genome (32), our current efforts to expand MADM to other chromosomes should enable detailed functional analyses of many more genes *in vivo*.

Materials and Methods

Generation of MADM Knockout Mice. GR/RG;Cre (WT-MADM), *p27* GR/RG;Cre (GR-MADM), and *p27* RG/GR;Cre (RG-MADM) mice were generated as described in SI Fig. 5*B*. *p27* heterozygote mice were obtained from The Jackson Laboratory, Bar Harbor, ME (9). Hprt-Cre (13) was used throughout the study except in the cerebellar mutant/WT ratio quantification (Fig. 2 *D* and *D′*), where Wnt1-Cre (33) was used. Genotyping of the RG and GR transgenes, the *p27* null allele, and Cre transgenes was performed by PCR as described (7, 9). The studies were performed in mixed background mice generated by crossing Cre transgene (129S1, B6, CBA), *p27* heterozygote (129S4), and MADM mice (129S1, CD-1) of varying genetic backgrounds.

Tissue Preparation and Histology. All animal procedures were based on animal care guidelines approved by Stanford University's Administrative Panels on Laboratory Care (A-PLAC). Brain and liver tissues were isolated from anesthetized mice perfused with 4% paraformaldehyde (PFA) in 0.1 M PBS, fixed overnight in 4% PFA at 4°C, cryoprotected in 30% sucrose, and embedded in optimal cutting temperature (OCT). For cell cycle stage analysis, 60 mg/kg BrdU was administered by i.p. injection 1–3 h before sacrifice. Tissues were sectioned at 10- to 30-μm thickness. Cryosections were treated for immunofluorescence and processed for confocal imaging as described (7). GFP was detected by anti-GFP primary antibody (chicken, 1:500, Cat. no. GFP-1020; Aves Labs, Tigard, OR). MYC-tagged DsRed2 was detected by anti-MYC primary antibody (goat, 1:200, Cat. no. 600-338; Novus Biologicals, Littleton, CO). Primary antibodies against the following proteins were also used: p27kip1 (mouse, 1:100, Cat. no. 610242; BD Transduction Laboratories, Lexington, KY), Ki67 (rabbit, 1:500, Cat. no. NCL-Ki67p; Vision Biosystems, Norwell, MA), BrdU (rat, 1:250, Cat. no. OBT0030; Accurate Chemical, Westbury, NY), phospho-Histone 3 (Ser-10; rabbit, 1:250, Cat. no. 06-570; Upstate Biotechnology, Lake Placid, NY), cleaved caspase-3 (Asp-175, rabbit, 1:50, Cat. no. 9664S; Cell Signaling Technology, Beverly, MA), NeuN (mouse, 1:250, Cat. no. MAB377; Chemicon, Temecula, CA), and GABA-A receptor α6 (rabbit, 1:500, Cat. no. AB5610; Chemicon). Secondary antibodies were obtained from Jackson ImmunoResearch, West Grove, PA.

Quantification Methods. Granule cell expansion (Fig. 2 *D* and *D′*) was quantified from P22 cerebella of *p27* GR/RG;Wnt1-Cre mice. Wnt1 is expressed in an anteroposterior gradient in cerebellar progenitors (33). The Wnt1-Cre line leads to sparser labeling of granule cells than Hprt-Cre, permitting more accurate quantification. Unbiased sampling was performed by counting all green and red cells in lobule VIII from 5–10 nonadjacent 20-μm sagittal sections (150–250 μm apart) across the mediolateral span of the cerebellum (n = 9 for WT-MADM and n = 6 for GR-MADM) under fluorescence microscopy. Hepatocyte expansion (Fig. 2 *E* and *E′*) was determined by quantification of all cells in hepatocyte twinspots (n = 20–30 per genotype from 2+ mice), defined as clusters of adjacent green and red cells at least 300 μm away from other green or red cells. Twinspots never spanned >275 μm in diameter (average of 128 μm). To ensure that twinspot quantifications were unbiased, all green and red cells were counted from >5 nonadjacent 25-μm sections (150–250 μm apart) of the left and right main liver lobes (n = 3–4). "Mutant"-to-WT ratios for WT-MADM and GR-MADM/RG-MADM were 1.15 ± 0.64 SEM and 2.73 ± 0.84 SEM, respectively, in line with twinspot quantifications (Fig. 2*E′*). Geometric means in original scale were used throughout statistical analyses of ratios. Cell cycle stage profiling (Fig. 3) was performed by counting the proportion of 30–70 green, red, and yellow cells per P4 GR-MADM cerebellum that were labeled with BrdU or pH3 by using 1-μm optical sectioning by confocal microscopy (n = 4). Cell cycle exit timing of granule cells (Fig. 4*B*) was quantified by counting all green and red cells in the EGL and IGL separately in 10–12 nonadjacent 30-μm sagittal sections (150–250 μm apart) across the mediolateral span of P4 GR-MADM cerebella (n = 10).

Statistics. Statistical comparison of mutant/WT ratios of WT-MADM, GR-MADM, and RG-MADM granule cells (n = 9 for WT-MADM, n = 6 for GR-MADM; Fig. 2*D′*) and hepatocyte twinspots (n = 21 for WT-MADM, n = 29 for GR-MADM, n = 20 for RG-MADM; Fig. 2*E′*) was performed by permutation analysis with 100,000 iterations (Matlab). Comparison of EGL/IGL of red and green granule cells from P4 GR-MADM mice (Fig. 4*B*) was performed by permutation analysis with 10,000 iterations (Matlab). The extent of correlation between mutant/WT ratios and hepatocyte twinspot size (n = 49, Fig. 4*D*) was determined by linear

regression analysis (Excel) and computation of the correlation coefficient of variation and P value. The standard for significance in all statistical analyses was $P < 0.05$.

We thank L. Attardi, G. Barsh, J. S. Espinosa, O. Schuldiner, M. Scott, and B. Tasic for critical reading of the manuscript; W. Zhong for technical support; and W. Wang and A. Bradley for sharing unpublished results and for coordinating submission. This research was supported by National Institutes of Health Grant R01-NS050835 (to L.L.). M.D.M. was supported by a Howard Hughes Medical Institute (HHMI) Research Training Fellowship for Medical Students and a Stanford Medical Scholars Research Fellowship. L.L. is an HHMI Investigator.

1. Hanahan D, Weinberg RA (2000) *Cell* 100:57–70.
2. Sherr CJ (2004) *Cell* 116:235–246.
3. Knudson AG, Jr (1971) *Proc Natl Acad Sci USA* 68:820–823.
4. Jonkers J, Berns A (2002) *Nat Rev Cancer* 2:251–265.
5. Novak A, Guo C, Yang W, Nagy A, Lobe CG (2000) *Genesis* 28:147–155.
6. Holzenberger M, Lenzner C, Leneuve P, Zaoui R, Hamard G, Vaulont S, Bouc YL (2000) *Nucleic Acids Res* 28:E92.
7. Zong H, Espinosa JS, Su HH, Muzumdar MD, Luo L (2005) *Cell* 121:479–492.
8. Sherr CJ, Roberts JM (1995) *Genes Dev* 9:1149–1163.
9. Fero ML, Rivkin M, Tasch M, Porter P, Carow CE, Firpo E, Polyak K, Tsai LH, Broudy V, Perlmutter RM, *et al.* (1996) *Cell* 85:733–744.
10. Lloyd RV, Erickson LA, Jin L, Kulig E, Qian X, Cheville JC, Scheithauer BW (1999) *Am J Pathol* 154:313–323.
11. Tsihlias J, Kapusta L, Slingerland J (1999) *Annu Rev Med* 50:401–423.
12. Wang VY, Zoghbi HY (2001) *Nat Rev Neurosci* 2:484–491.
13. Tang SH, Silva FJ, Tsark WM, Mann JR (2002) *Genesis* 32:199–202.
14. Miyazawa K, Himi T, Garcia V, Yamagishi H, Sato S, Ishizaki Y (2000) *J Neurosci* 20:5756–5763.
15. Zhao R, Duncan SA (2005) *Hepatology* 41:956–967.
16. Michalopoulos GK, DeFrances MC (1997) *Science* 276:60–66.
17. Huang W, Ma K, Zhang J, Qatanani M, Cuvillier J, Liu J, Dong B, Huang X, Moore DD (2006) *Science* 312:233–236.
18. Sage J, Miller AL, Perez-Mancera PA, Wysocki JM, Jacks T (2003) *Nature* 424:223–228.
19. Zheng JY, Wang WZ, Li KZ, Guan WX, Yan W (2005) *World J Gastroenterol* 11:7072–7077.
20. Krueger BK, Burne JF, Raff MC (1995) *J Neurosci* 15:3366–3374.
21. Mitsuhashi T, Aoki Y, Eksioglu YZ, Takahashi T, Bhide PG, Reeves SA, Caviness VS, Jr (2001) *Proc Natl Acad Sci USA* 98:6435–6440.
22. de Nooij JC, Letendre MA, Hariharan IK (1996) *Cell* 87:1237–1247.
23. Durand B, Fero ML, Roberts JM, Raff MC (1998) *Curr Biol* 8:431–440.
24. Kawauchi T, Chihama K, Nabeshima Y, Hoshino M (2006) *Nat Cell Biol* 8:17–26.
25. Chen P, Segil N (1999) *Development (Cambridge, UK)* 126:1581–1590.
26. Tong W, Kiyokawa H, Soos TJ, Park MS, Soares VC, Manova K, Pollard JW, Koff A (1998) *Cell Growth Differ* 9:787–794.
27. Dyer MA, Cepko CL (2001) *J Neurosci* 21:4259–4271.
28. Wilson JC, Zhu JJ, Black PM (1999) *J Neurooncol* 44:35–39.
29. Yuste R, Konnerth A (2005) *Imaging in Neuroscience and Development: A Laboratory Manual* (Cold Spring Harbor Lab Press, Cold Spring Harbor, NY).
30. Mehta AD, Jung JC, Flusberg BA, Schnitzer MJ (2004) *Curr Opin Neurobiol* 14:617–628.
31. Xu T, Rubin GM (1993) *Development (Cambridge, UK)* 117:1223–1237.
32. Austin CP, Battey JF, Bradley A, Bucan M, Capecchi M, Collins FS, Dove WF, Duyk G, Dymecki S, Eppig JT, *et al.* (2004) *Nat Genet* 36:921–924.
33. Danielian PS, Muccino D, Rowitch DH, Michael SK, McMahon AP (1998) *Curr Biol* 8:1323–1326.